



The Effects of Ferromagnetic Disks on AC Losses in HTS Pancake Coils with Nonmagnetic and Magnetic Substrates

Mengdie Niu^{1,2} · Huadong Yong^{1,2} · Jing Xia³ · Youhe Zhou^{1,2}

Received: 24 March 2018 / Accepted: 15 May 2018 / Published online: 29 May 2018
© Springer Science+Business Media, LLC, part of Springer Nature 2018

Abstract

Performance improvement of high-temperature superconducting (HTS) pancake coil is of paramount importance for its application in electrical facilities. In this paper, the utilization of ferromagnetic disks including weak magnetic material and strong magnetic material is investigated through numerical simulations for the aim of reducing the AC loss. Both the nonmagnetic and magnetic substrates are considered for the rare-earth-barium-copper-oxide coated conductor tapes wounded into the pancake coil. In order to analyze the influences of ferromagnetic disks on the maximum allowable currents and AC losses of nonmagnetic substrate-based coil and magnetic substrate-based coil, a self-consistent model based on the **A**-formulation is adopted to calculate the critical current and a 2D axisymmetric model built on the **H**-formulations is established to calculate the AC loss. According to the simulation results, it is found that ferromagnetic disks especially the strong magnetic disk are slightly detrimental to the critical currents of the pancake coils. Nevertheless, the presence of large background field weakens the effects of ferromagnetic disks. The simulation results also indicate that strong magnetic disks achieve about 50% reduction of the AC loss in the nonmagnetic substrate-based coil, and the AC loss of the magnetic substrate-based coil can be increased or reduced with strong magnetic disks depending on the applied current amplitude. The utilization of strong magnetic disks leads to the enhancement of the AC loss in the magnetic substrate-based coil at lower current and to the reduction of it at larger current.

Keywords Pancake coil · Magnetic substrate · Ferromagnetic disk · Critical current · AC loss

1 Introduction

Owing to the impressive improvements on the conductor length, electrical and mechanical performances over the past decades, the second-generation high-temperature

superconductor has become more and more promising for practical applications such as superconducting electrical machines [1], energy storage systems [2, 3], and magnets and cables [4, 5]. Rare-earth-barium-copper-oxide (REBCO) coated conductor (CC) tape is composed of a REBCO superconducting thin film deposited on metallic substrates [6], and it is mainly composed of layers of superconductor, stabilizer and substrate [7]. Two highly textured materials are widely used for the substrate, i.e., Hastelloy (normal metal material) (SuperPower, Inc., www.superpower-inc.com) and Ni alloy material (weak magnetic material) (AMSC, www.amsc.com). Developing the pancake coils wound with REBCO CC tape is one of significant topics in large-scale superconducting applications [8, 9]. However, the performance of the pancake coils is usually limited by two important factors, i.e., the critical current and AC loss. The critical current and AC loss of the pancake coil directly determine the maximum allowable transport current and the coolant consumption. And, the overlarge AC loss would pose a challenge to maintain the safety

✉ Huadong Yong
yonghd@lzu.edu.cn
Jing Xia
power_xj@163.com

¹ Key Laboratory of Mechanics on Disaster and Environment in Western China, Ministry of Education of China, Lanzhou University, Lanzhou, 730000 Gansu, People's Republic of China
² Department of Mechanics and Engineering Sciences, College of Civil Engineering and Mechanics, Lanzhou University, Lanzhou, Gansu 730000, People's Republic of China
³ Center for Fusion Energy Science and Technology, China Academy of Engineering Physics, Beijing 100088, People's Republic of China

and stability of the superconducting devices. Thus, in order to realize the optimization design and low-cost operation, it is extremely meaningful to investigate the critical current and AC loss of the pancake coils.

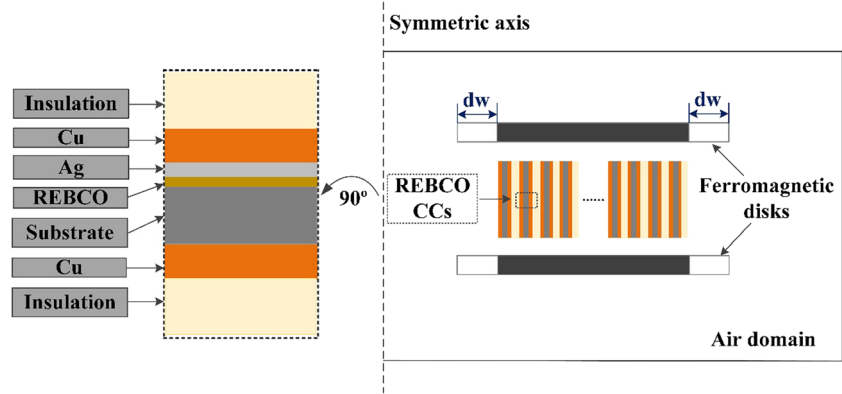
Different research groups have come up with some innovative and particular ways to lower the AC loss, such as twisted wires [10], striated HTS-coated conductors [11], and Robel cable [12, 13]. Although the proposed methods have been proved to be effective in decreasing the losses, these methods change the conventional configuration of superconducting tape, affecting the mechanical property of the superconductor as well as increasing the cost of processing and manufacturing. The striated tape even introduces local defects [14]. On the other hand, without changing the original configuration of tape, the reasonable arrangement of ferromagnetic materials is a simple and effective approach to reduce the AC loss [15]. Ferromagnetic materials can attract the magnetic flux and thus change the way of the magnetic flux penetration [16–19]. The AC loss of the superconductor can be higher or lower, which relies on the exact geometric dimensions, shape, position, and ferromagnetism of ferromagnetic materials. Different ferromagnetic materials are adopted in superconducting devices for lowering the AC loss, such as ferromagnetic coat, iron core, and magnetic flux diverter [19–25]. A horseshoe coat for HTS CC tape [21, 22] and a C-shape coat covering partial elliptical tape edges [23] could significantly reduce the AC loss in the superconducting part, while the completely covered coating for Bi2223 multifilamentary tapes is detrimental to its performance [24]. Stacked HTS tapes embedded in an iron core would suffer more AC transport loss in comparison to that without an iron core [25]. An iron core inserted in the center of HTS coils doubles the AC loss of coils, which can be interpreted by a fringe magnetic field and the magnetic mirror effect [26]. Nevertheless, magnetic flux diverter works well on suppressing the AC losses for staked HTS tapes and HTS pancake coils [15, 27, 28]. Magnetic flux diverter positioned on both sides of stacked HTS tapes could largely lower the AC loss in stacked HTS tapes with and without magnetic substrates, and a larger reduction could be achieved with the utilization of a thicker (1 mm) and stronger magnetic material [15]. Ref. [15] pointed out that the magnetic flux diverter with high saturation field and low saturated hysteretic loss would be the optimal choice for AC loss reduction. Later, the use of flux diverter was extended to improve the performance on the critical current and AC loss for HTS pancake coils. The magnetic flux diverter in the form of two identical disks was placed symmetrically on both sides of HTS pancake coils. The flux diverter does decrease transport AC loss even when considering the ferro-

magnetic loss of magnetic flux diverter, and it exerts small negative influence on DC properties [28]. Further optimization design of the flux diverter in stacked tapes and HTS pancake coils was developed, getting a conclusion that the diverter with suitable geometrical size, shape, and location suppresses the AC loss significantly [27, 29].

Extensive research studies on the superconducting tapes with magnetic substrates have been carried out, and these research results indicated that the magnetic substrates can change the magnetic field distribution around the superconducting tapes, lower the critical current, and increase the AC loss in some cases [30–32]. As for the pancake coils wound by a coated conductor tape with magnetic substrates, numerous investigations showed that magnetic substrates would cause larger AC loss due to the increased local magnetic field in the superconductor [33–37]. However, a detailed comparative study was conducted on two pancake coils with nonmagnetic and magnetic substrates. The experimental results indicated that, unlike single tape [38] and stacked tapes [39], two coils experienced roughly similar AC loss [34]. The influences of magnetic substrate on the AC loss of HTS pancake coils can be divided into two parts. While contributing an additional ferromagnetic hysteretic loss, the magnetic substrate also changes the magnetic flux penetration and thus influences AC loss in the superconductor. However, to our best knowledge, few references have reported the effect of magnetic flux diverter on the AC loss of HTS pancake coils with magnetic substrates.

In this paper, we attach two ferromagnetic disks to both sides of a pancake coil as the magnetic flux diverter. Different ferromagnetic materials including a weak magnetic Ni alloy material and a strong magnetic Ni alloy material used for the diverter are explored to analyze the ferromagnetism effect on performance of HTS pancake coils. Pancake coils wound by coated conductor tapes with Hastelloy substrate and weak magnetic Ni alloy substrate are considered for comparison. The influences of magnetic flux diverter on the characteristics with respect to the critical current and AC loss of pancake coils are studied by means of the numerical simulations. Section 2 presents a self-consistent model used to calculate the critical current of the pancake coils under different external fields. The magnetic field-dependent critical current density is also taken into account for accurate estimation. Section 3 introduces a **H**-formulation finite element model to analyze the transport AC loss of pancake coils under different fixed background fields. A comprehensive understanding about the influences of magnetic flux diverter on the AC loss of pancake coil is given. Section 4 summarizes the results.

Fig. 1 Two-dimensional axisymmetric model for the 50-turn REBCO pancake coil with ferromagnetic disks of thickness 1 mm placed on both sides. And, the value of dw is specified as 0 mm in the following calculations without a special instruction. The left image details the internal layer components of the coated conductor



2 DC Properties

2.1 Self-Consistent Model

The critical current density is noted as J_ϕ due to the transport current flowing along an annular direction, and the magnetic field has two nonzero components H_r and H_z ; a 2D axisymmetric model is constructed to solve the electromagnetic behaviors of the REBCO pancake coil, in which the real geometric dimensions are taken into account. The magnetic flux diverters are placed symmetrically on both sides of the pancake coil, and its real thickness is about 1 mm, the same as the axial spacing between the diverter and coil. Considering the particular shape of magnetic diverter, the diverter is regarded as a ferromagnetic disk in the following statement. The 2D simplified model is shown in Fig. 1, and the corresponding geometrical parameters are listed in Table 1 [28, 40].

When we study DC properties of REBCO pancake coils, the self-field induced by steady current is a static field. Therefore, the time-dependent Maxwell equations degrade into the static formulations. A self-consistent model based on the time-independent Maxwell equations was proposed

Table 1 Geometric parameters of the model

Parameter	Definition	Value
w (mm)	Tape width	4
t_{Ins} (μm)	Insulation layer thickness	200
t_{Cu} (μm)	Copper layer thickness	40
t_{Ag} (μm)	Silver layer thickness	2
t_{SC} (μm)	Superconducting layer thickness	1
t_{Subs} (μm)	Substrate layer thickness	50
D (μm)	Unit cell thickness	293
r_i (mm)	Inner radius of the coil	30

by Zermeño et al. [45, 46], which has been validated to be quite effective on estimating the critical current for different superconducting devices [47]. Here, we employ it to evaluate the critical current of REBCO pancake coils, and a brief description with respect to this model is given as follows.

The self-consistent model is based on the **A**-formulation. The magnetic vector potential **A** serves as the state variable, and the governing electromagnetic equation is formulated as

$$\nabla \times \frac{1}{\mu} \nabla \times \mathbf{A} = \mathbf{J} \tag{1}$$

where **A** and **J** stand for the magnetic vector potential and the current density vector, respectively. μ is the magnetic permeability defined as the product of the vacuum magnetic permeability ($\mu_0 = 4\pi \times 10^{-7}$ H/m) and the

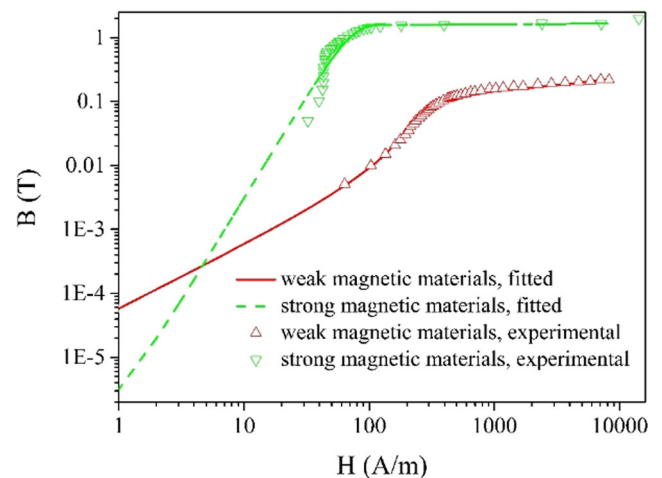


Fig. 2 The initial fitting magnetization curves for two ferromagnetic materials at 77 K and $f = 50$ Hz. The green solid line represents weak magnetic Ni alloy material, and the red dashed line represents strong magnetic Ni alloy material. The experimental data is from the literature [48]

relative magnetic permeability (μ_r). Here, μ_r is equal to 1 except for ferromagnetic materials. The relative magnetic permeability of ferromagnetic materials is dependent on the external magnetic field [48]. The magnetic flux density (\mathbf{B}) and the field intensity (\mathbf{H}) have a nonlinear relationship shown in Fig. 2 as $\mathbf{B} = \mu_0\mu_r\mathbf{H}$ for ferromagnetic materials [39, 49]. The analytical fitting functions on the relative permeability of both ferromagnetic materials are given in the following section.

The critical current density depends on the local magnetic field and temperature. Here, we solely take the anisotropy of $J_c(B)$ into account as a result of the negligible change on the temperature field. An elliptical formulation [44] shown as (2) is to observe the qualitative features of REBCO tapes. The real tapes present more complex anisotropies.

$$J_c(B_{\parallel}, B_{\perp}) = \frac{J_{c0}}{\left[1 + \sqrt{(kB_{\parallel})^2 + B_{\perp}^2/B_c}\right]^{\alpha}} \quad (2)$$

where B_{\parallel} and B_{\perp} represent the local magnetic flux density components parallel and perpendicular to the tape surface, respectively. The value of J_{c0} , k , B_c , and α is given in Table 2 [40–44].

The well-known power law is used to describe the continuous E – J relationship, i.e.,

$$E(J) = E_c \frac{J}{J_c(B)} \left| \frac{J}{J_c(B)} \right|^{n-1} \quad (3)$$

where E_c is the reference electrical field taken as $1 \mu\text{V}/\text{cm}$ in this paper, $J_c(B)$ is the critical current density related with the external field, and n is the flux creep exponent. Moreover, an auxiliary variable denoted by P is introduced to express nonlinear E – J relationship

$$P = \frac{J}{J_c(B)} = \frac{E}{E_c} \left| \frac{E}{E_c} \right|^{\frac{1}{n}-1} \quad (4)$$

Table 2 Physical properties of REBCO CCs

Parameter	Definition	Value
E_c (V/m)	Critical current criterion	1.0×10^{-4}
n	Power law exponent	38
J_{c0} (A/m ²)	Kim model parameter	2.8×10^{10}
B_c (mT)	Kim model parameter	42.65
k	Kim model parameter	0.29515
α	Kim model parameter	0.7
ρ_{Ins} ($\Omega \cdot \text{m}$)	Insulation resistivity	1
ρ_{Cu} ($\text{n}\Omega \cdot \text{m}$)	Copper resistivity	1.97
ρ_{Ag} ($\text{n}\Omega \cdot \text{m}$)	Silver resistivity	2.7
$\rho_{\text{Hastelloy}}$ ($\mu\Omega \cdot \text{m}$)	Hastelloy resistivity	1.25
ρ_{fe} ($\mu\Omega \cdot \text{m}$)	Ferromagnetic material resistivity	0.26

where P is uniform over the cross section of each turn in the DC case due to the uniform distribution of \mathbf{E} . Each turn carries the same current (I_0) and thereby has a constant P_i defined as follows:

$$P_i = I_0 / \int_{\Omega_i} J_c(B) ds \quad (5)$$

where Ω_i denotes the cross section of the i th turn. I_c is determined by the max criterion [45]; i.e., the critical current corresponds to the value of transport current when $\max\{P_i\}_{i=1,2,\dots,50} = 1$.

The self-consistent model is implemented by means of the AC/DC module in the finite element software COMSOL (COMSOL, Inc., <http://www.comsol.com>), which provides the solver to solve Ampere’s Law for the magnetic vector potential. The execution process of determining the critical current is illustrated in Fig. 3.

2.2 The Critical Current of the Pancake Coils

Five different configurations are considered for the pancake coils. “NMNF” denotes the nonmagnetic substrate-based coil without ferromagnetic disks; “NMWF” denotes the nonmagnetic substrate-based coil with weak magnetic

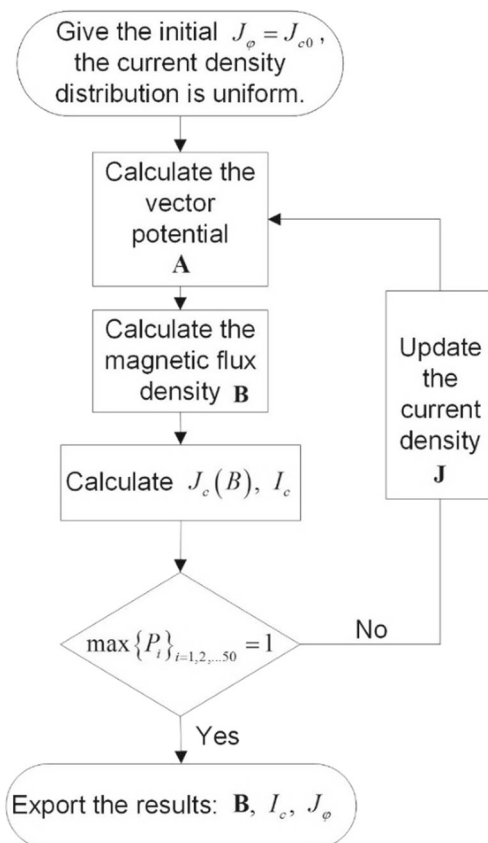


Fig. 3 Schematic diagram of self-consistent model calculating the critical current

Table 3 The critical current of pancake coils for five configurations under different axial background fields, $B_{app} = 0, 0.5,$ and $1T$

Configurations	NMNF	NMWF	NMSF	WMWF	WMSF
$I_c[A], B_{app} = 0$	60.67	58.08	49.59	57.41	50.74
$I_c[A], B_{app} = 0.5T$	35.84	34.96	32.02	35.58	33.28
$I_c[A], B_{app} = 1T$	25.33	24.97	23.47	25.24	24.5

disks; “NMSF” denotes the nonmagnetic substrate-based coil with strong magnetic disks; “WMWF” denotes the magnetic substrate-based coil with weak magnetic disks; “WMSF” denotes the magnetic substrate-based coil with strong magnetic disks.

Executing the COMSOL program of self-consistent model, we calculate the critical current for 50-turn REBCO pancake coils in self-field and external-field conditions. The critical current for nonmagnetic substrate-based coil without ferromagnetic disks is taken as a reference. Table 3 gives the calculated critical current for five configurations under different axial background fields, $B_{app} = 0, 0.5,$ and $1T$. Figure 4 presents a comparison of the critical current reduction for those coils. The reduction in the critical current is expressed as a percentage of the reference. It is found that the utilization of ferromagnetic disks slightly reduces the critical current of pancake coils. The critical current reduction is particularly pronounced when using the strong magnetic disk. And, the largest reduction corresponds to the nonmagnetic substrate-based coil with strong magnetic disk in self-field condition, achieving approximately 18%. The critical current reduction should attribute to the enhancement of the weakest turn’s field, and the innermost turn is found to be the weakest turn, as shown

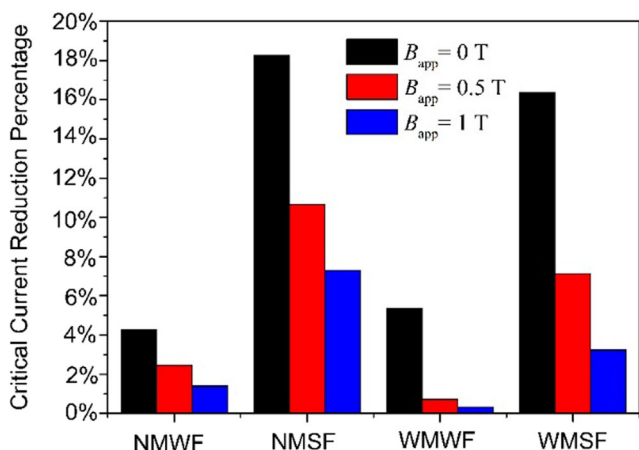


Fig. 4 The reduction in the critical current for nonmagnetic substrate-based coil and magnetic substrate-based coil using weak and strong magnetic disks in the conditions of $B_{app} = 0, 0.5,$ and $1T$. The reduction of critical current is expressed as the percentage of the critical current of nonmagnetic substrate-based coil without ferromagnetic disks

in Fig. 5. The field of innermost turn is strengthened by the strong magnetic disk, and thus the critical current declines.

Figure 6 shows the critical current for all pancake coils varies with the axial background field. When the external field increases from 0.01 to $1T$, the ferromagnetic disks lead to a greater decrease in the critical current of nonmagnetic substrate-based coil than that of magnetic substrate-based coil. When the axial background field exceeds $2T$, the deviations among the critical currents for all pancake coils disappear gradually, which is because the influences of saturated ferromagnetic disks and magnetic substrates can be neglected in comparison to the contribution of the background field, and therefore, the critical current reduction is driven by the larger background field.

3 AC Analysis

3.1 H-Formulation

The AC properties of REBCO pancake coils for the five different configurations are studied under the external axial field conditions with $B_{app} = 0$ and $0.5 T$. The finite element method based on the **H**-formulation [50–54] is used to model the electromagnetic behaviors of pancake coils and calculate the AC losses.

The 2D axisymmetric **H**-formulated Maxwell equations have the following form:

$$\begin{bmatrix} -\frac{1}{r} \frac{\partial r E_\varphi}{\partial z} \\ \frac{1}{r} \frac{\partial r E_\varphi}{\partial r} \end{bmatrix} + \mu_0 \begin{bmatrix} \frac{\partial \mu_r H_r}{\partial r} \\ \frac{\partial \mu_r H_z}{\partial t} \end{bmatrix} = \begin{bmatrix} 0 \\ 0 \end{bmatrix} \tag{6}$$

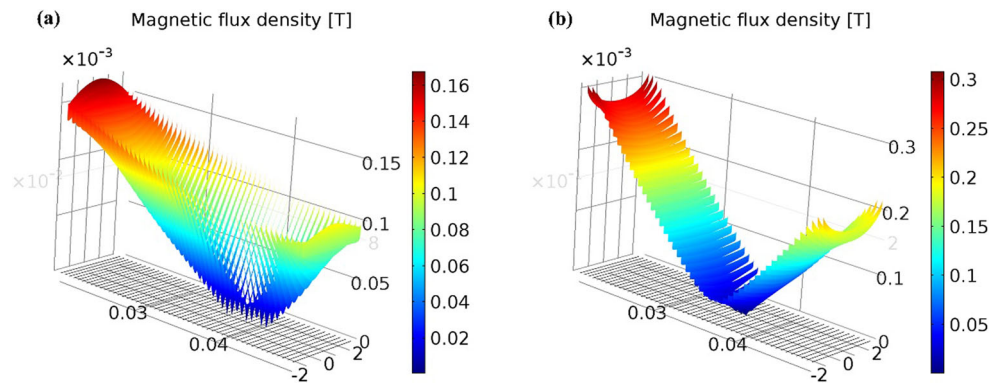
$$\frac{\partial H_r}{\partial z} - \frac{\partial H_z}{\partial r} = J_\varphi \tag{7}$$

where E_φ represents the annular electric field component and E_φ is equal to the product of resistivity (ρ) and annular current density (J_φ) with $\rho = \text{const}$ for the normal conductor, and $\rho = \frac{E_c}{J_c(B)} \left| \frac{J_\varphi}{J_c(B)} \right|^{n-1}$ for the superconductor. H_r and H_z are the state variables, denoting the radial and axial magnetic fields, respectively. Substituting Ampere’s Law (7) into (6), we get the governing equations

$$\begin{bmatrix} -\frac{1}{r} \frac{\partial r \rho \times (\partial H_r / \partial z - \partial H_z / \partial r)}{\partial z} \\ \frac{1}{r} \frac{\partial r \rho \times (\partial H_r / \partial z - \partial H_z / \partial r)}{\partial r} \end{bmatrix} + \mu_0 \mu_r \begin{bmatrix} \frac{\partial H_r}{\partial t} \\ \frac{\partial H_z}{\partial t} \end{bmatrix} + \mu_0 \frac{\partial \mu_r}{\partial t} \begin{bmatrix} H_r \\ H_z \end{bmatrix} = \begin{bmatrix} 0 \\ 0 \end{bmatrix} \tag{8}$$

where μ_r stands for the relative magnetic permeability and is set to 1 for the layers of copper, silver, superconductor, nonmagnetic substrate, and insulation. For the ferromagnetic materials, μ_r is considered as a function related to the magnitude of magnetic field vector, namely $\mu_r(H)$, in

Fig. 5 The magnetic flux density distribution in superconducting layers for nonmagnetic substrate-based coil with and without strong magnetic disks in self-field. **a** The case without ferromagnetic disk. **b** The case with strong magnetic disks



which H refers to the numerical value: $\sqrt{H_r^2 + H_z^2}$. The relative permeability of weak magnetic material served as ferromagnetic disks or substrate has the following form [49]:

$$\mu_r(H) = 1 + \left\{ 1 - \exp \left[-(a_0 H)^{b_0} \right] \right\} \times (c_0 H)^{d_0} + e_0 \exp \left[-(f_0 H)^{g_0} \right] \quad (9)$$

where $a_0 = 0.0034, b_0 = 2.5, c_0 = 2.9 \times 10^{-6}, d_0 = -0.81, e_0 = 45, f_0 = 0.0083,$ and $g_0 = 2.5$. The magnetic field-dependent relative magnetic permeability of strong magnetic material served as ferromagnetic disks is as follows [39]:

$$\mu_r(H) = 1 + \left\{ 1 - \exp \left[(a_1 H)^{b_1} \right] \right\} \times (c_1 H)^{d_1} \quad (10)$$

where $a_1 = -0.014, b_1 = 3.2, c_1 = 7.24 \times 10^{-7},$ and $d_1 = -0.99$. It should be noted that the relative permeability of ferromagnetic materials is time-dependent due to the time-dependent essence of $H(t)$. Thus, the last term on the left side of (8) cannot be neglected. Expanding the first

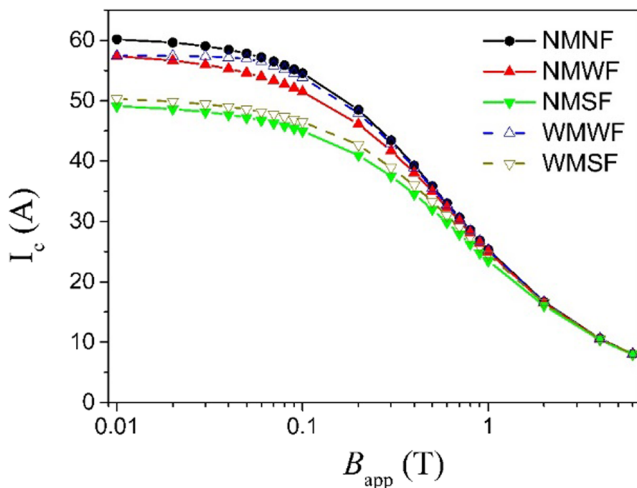


Fig. 6 The critical current for pancake coils with five configurations as a function of axially applied field

derivative of relative permeability on time would give an integrated comprehension on (8).

$$\frac{\partial \mu_r(H)}{\partial t} = \left(\frac{H_r}{H} \frac{d\mu_r(H)}{dH} \right) \frac{\partial H_r}{\partial t} + \left(\frac{H_z}{H} \frac{d\mu_r(H)}{dH} \right) \frac{\partial H_z}{\partial t} \quad (11)$$

The general PDE module of the FE software COMSOL is employed to solve the partial differential equation (8). Pointwise constraint is adopted to control the applied transport current, i.e., $I(t) = I_0 \sin(2\pi ft)$ with $f = 50$ Hz. The current amplitude ranges from $0.1I_c$ to $0.9I_c$. When the axially background field exists, $H_z(t) = H_0/t_{\text{ramp}} \times t (t \leq t_{\text{ramp}})$ and $H_z(t) = H_0 (t > t_{\text{ramp}})$ are applied on the outer boundary of the model by the Dirichlet boundary condition.

Once the current density distribution and the magnetic field distribution in the pancake coil are obtained, the eddy current loss in metal layers and the magnetic hysteresis loss in the superconducting layer can be calculated by this formula

$$Q = \int_{T/2}^{3T/2} dt \int_{\Omega} 2\pi r E_{\varphi} J_{\varphi} ds \quad (12)$$

where Ω denotes the cross section of the layers of metals and superconductor. For ferromagnetic materials, there exists an additional hysteresis loss except for eddy current loss. With respect to the two types of ferromagnetic materials, empirical formulas of hysteresis loss density (with the unit of $J/m^3/\text{cycle}$) associated with the maximum magnetic flux density (B_m) during 1 cycle are adopted. Equations (13) and (14) represent the cases of the weak magnetic Ni alloy material [49] and strong magnetic Ni alloy material [39], respectively

$$Q_W^{\text{fc}}(B_m) = \begin{cases} \alpha_0 B_m^{\beta_0}, & B_m \leq 0.164 \text{ T} \\ e_1 \{ 1 - \exp[-(f_1 B_m)^{g_1}] \}, & B_m > 0.164 \text{ T} \end{cases} \quad (13)$$

$$Q_S^{\text{fc}}(B_m) = \begin{cases} \alpha_1 B_m^{\beta_1}, & 0.1 \text{ T} \leq B_m \leq 1.53 \text{ T} \\ h_1 \{ 1 - \exp[-(k_1 B_m)^{m_1}] \}, & B_m > 1.53 \text{ T} \end{cases} \quad (14)$$

Here, $\alpha_0 = 4611.4$, $\beta_0 = 1.884$, $e_1 = 210$, $f_1 = 6.5$, $g_1 = 4$, $\alpha_1 = 171.2$, $\beta_1 = 1.344$, $h_1 = 375$, $k_1 = 0.7107$, and $m_1 = 6.787$.

3.2 AC Loss

For convenience of expression, we use Q_{sc} , Q_{cu} , Q_{disk} , Q_{sub} , Q_{coil} , and Q_{tot} to denote the AC loss in superconducting layers, the eddy current loss in Cu stabilizers, the hysteresis loss in ferromagnetic disks, the hysteresis loss in magnetic substrates, the AC loss in the pancake coil, and the overall loss of the configuration, respectively. Noting that Q_{coil} is the sum of losses in the layers of CC tapes, and the eddy current loss in ferromagnetic substrate is omitted. Q_{tot} is the overall loss of the coil configuration, including the AC loss in the coil (Q_{coil}) and the hysteresis loss in the ferromagnetic disks (Q_{disk}). To be mentioned, the eddy current loss in ferromagnetic materials is not taken into account as a result of negligible part compared to the hysteresis loss.

Firstly, the AC loss of the pancake coils for five configurations is studied in the self-field condition. For figuring out the distribution of losses among different components, the loss of component as a function of applied current amplitude is shown in Fig. 7 for the pancake coils with three representative configurations, i.e., nonmagnetic substrate-based coil with and without strong magnetic disks and magnetic substrate-based coil with strong magnetic disks.

Figure 7a demonstrates the case of nonmagnetic substrate-based coil without ferromagnetic disks. One can see that the AC loss in superconducting layers is approximately equal to the total energy dissipation in the coil, and the curves for Q_{sc} and Q_{coil} are indistinguishable accordingly. Similar feature can be found for the nonmagnetic substrate-based coil with strong magnetic disks (see from Fig. 7b). Hence, the eddy current loss in metal layers can be ignored. Hysteresis loss in strong magnetic disks has a higher magnitude than the AC loss in the coil as the normalized current ($i < 0.5$). When the applied current gradually approaches the critical current, the hysteresis loss in strong magnetic disks tends to be saturated and it is 75% lower than the AC loss in the coil at $i = 0.8$. Thus, the strong magnetic disks used in nonmagnetic substrate-based coil contribute few losses to overall energy dissipation at larger current. For the magnetic substrate-based coil with strong magnetic disks (see from Fig. 7c), the hysteresis loss in substrates is higher than the losses in superconducting and metal layers when $i < 0.31$, occupying 60% of the AC loss in the coil at $i = 0.2$. With the increase of the applied current, the AC loss in superconducting layers gradually dominates the AC loss in the coil and occupies 90% of the AC loss in the coil at $i = 0.8$. This is because the weak Ni alloy material that

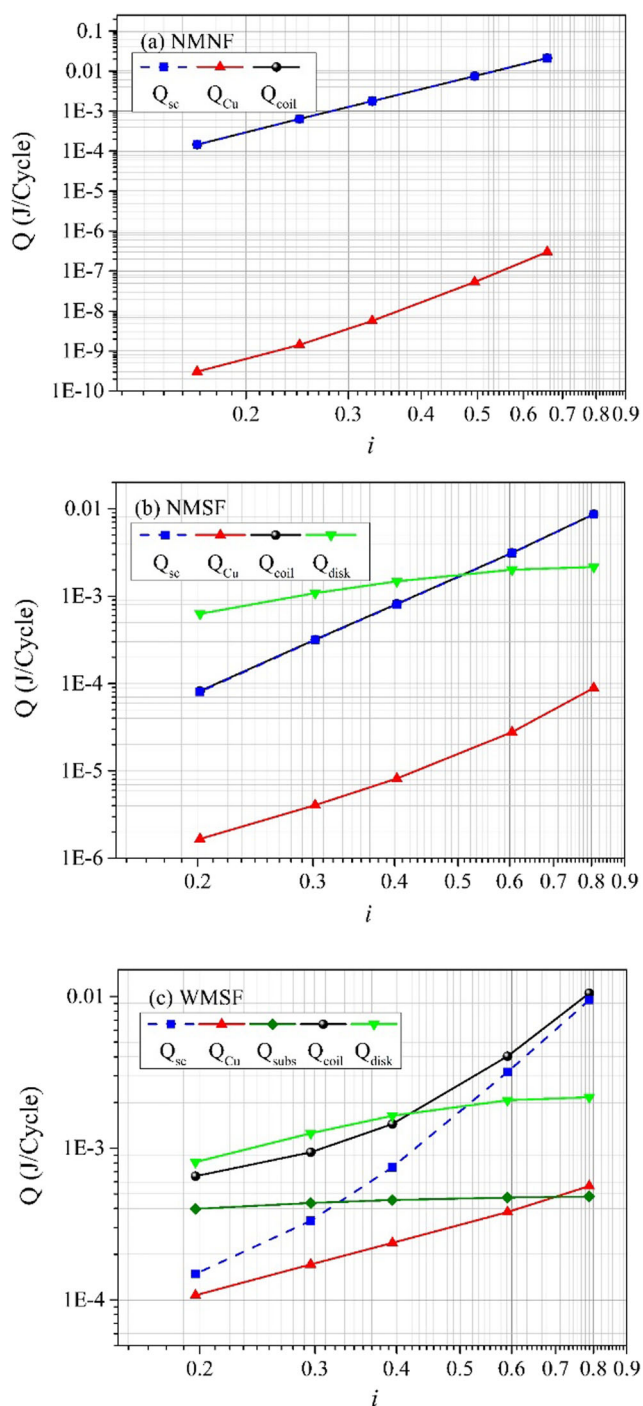


Fig. 7 The AC loss of REBCO pancake coils varies with the normalized applied current (i). **a** The nonmagnetic substrate-based coil without ferromagnetic disks (“NMNF”). **b** The nonmagnetic substrate-based coil with strong magnetic disks (“NMSF”). **c** The magnetic substrate-based coil with strong magnetic disks (“WMSF”). The current amplitude is normalized to the coil’s critical current. The Q_{sc} and Q_{coil} curves are indistinguishable in **a**, **b**

served as a substrate has a relatively low saturated field and the hysteresis loss of such substrate easily reaches the saturated value at low applied current. It is also notable that the

AC loss in the coil exceeds the hysteresis loss in strong magnetic disks when $i > 0.41$ and the hysteresis loss in strong magnetic disks is 80% lower than the AC loss in the coil at $i = 0.8$.

In order to further interpret the influences of ferromagnetic disks on the energy dissipation of the coil system, Fig. 8 gives a comparison on the losses of components for the pancake coils with five configurations, i.e., the non-magnetic substrate-based coil without ferromagnetic disks, the nonmagnetic substrate-based coil with weak and strong magnetic disks, and the magnetic substrate-based coil with weak and strong magnetic disks. The losses used for comparison include the AC loss in superconducting layers, the eddy current loss in copper layers, the AC loss in the coil, and the overall loss in the coil configuration. The nonmagnetic substrate-based coil without ferromagnetic disks is taken as the reference model in the following statement.

As can be seen from Fig. 8a, the AC loss in superconducting layers for the magnetic substrate-based coil with weak magnetic disks is highest among the five configurations. Three other configurations exhibit lower loss compared to the reference model. Moreover, the nonmagnetic substrate-based coil with strong magnetic disks and the magnetic substrate-based coil with strong magnetic disks undergo the same lowest AC loss in superconducting layers among the five configurations as $I_0 > 15$ A. The AC loss reduction in superconducting layers achieves 59.4% at $I_0 = 40$ A using the strong magnetic disks. Thus, whether for the nonmagnetic substrate-based coil or magnetic substrate-based coil, the utilization of strong magnetic disks with high saturation field achieves a pronounced reduction of the AC loss in superconducting layers. The detailed mechanism on that issue will be discussed in the next part.

The comparison on the eddy current loss in copper layers for the five configurations is shown in Fig. 8b. It is found that the ferromagnetic disks greatly increase the eddy current loss in copper layers for both nonmagnetic substrate-based coil and magnetic substrate-based coil. Due to the negligible eddy current loss in metal layers for nonmagnetic substrate-based coil, the AC loss reduction in nonmagnetic substrate-based coil caused by ferromagnetic disks (see from Fig. 8c) is approximately equal to the reduction of the AC loss in superconducting layers. The strong magnetic disks lead to a large AC loss reduction in nonmagnetic substrate-based coil, and the reduction of the AC loss in the coil achieves 59.3% at $I_0 = 40$ A compared to the reference model. As for the AC loss in magnetic substrate-based coil with weak magnetic substrates, it is higher than the AC loss in the reference model, as a result of increased AC loss in superconducting layers, increased eddy current loss in copper layers, and additional hysteresis loss in substrates. In addition, the AC loss in magnetic substrate-based coil with

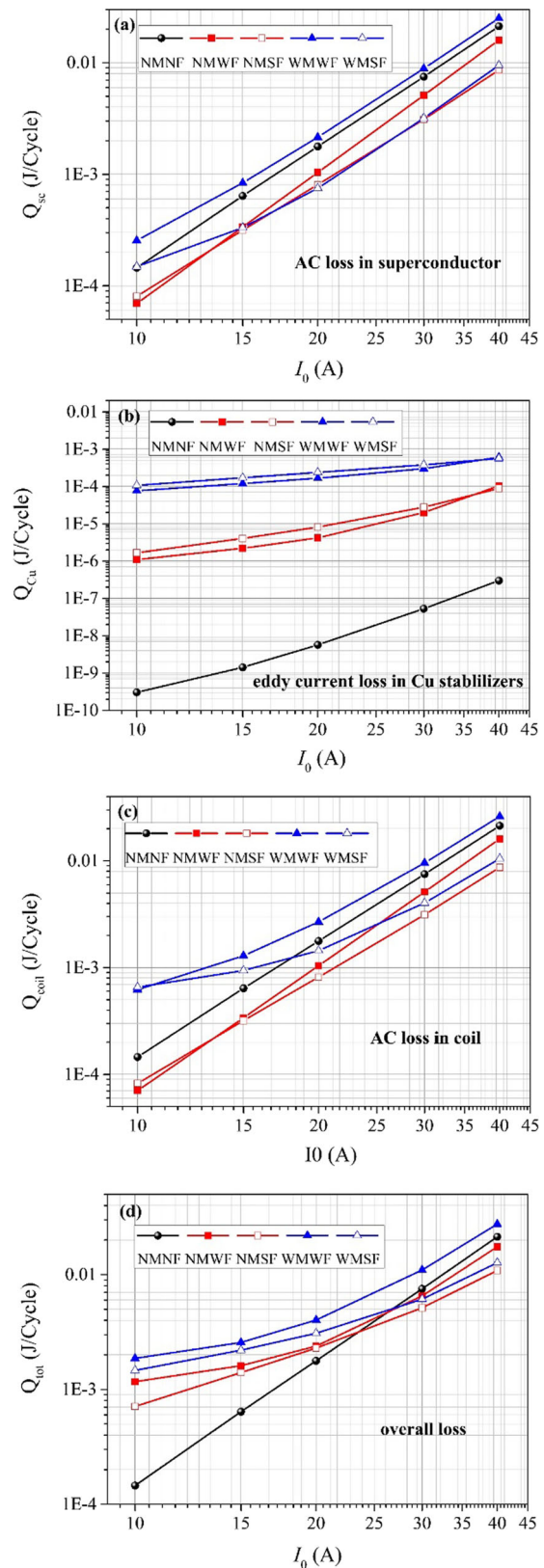


Fig. 8 Comparisons of losses of components in pancake coils for five configurations. **a** AC loss in superconducting layers. **b** Eddy current loss in Cu stabilizers. **c** AC loss of the pancake coil. **d** Overall loss of the configuration

strong magnetic disks is higher than the reference model as $I_0 > 17\text{A}$. This can be explained by the dominant hysteresis loss in substrates and significantly increased eddy current loss in copper layers at small current. As $I_0 > 17\text{A}$, the AC loss in magnetic substrate-based coil with strong magnetic disks becomes smaller than that in the reference model. The AC loss reduction caused by strong magnetic disks achieves 50.7% at $I_0 = 40\text{A}$. Therefore, strong magnetic disks perform well on reducing the AC loss of both nonmagnetic substrate-based coil and magnetic substrate-based coil at large current.

A comparison on the overall loss for five different configurations is shown in Fig. 8d, in which the hysteresis loss in ferromagnetic disks is included. It is found that the overall loss of the reference coil is the lowest as $I_0 < 24\text{A}$. This is because, as previously discussed, the additional hysteresis loss in ferromagnetic disks dominates the overall loss at small current. As the current amplitude becomes larger, except for the magnetic substrate-based coil with weak magnetic disks, the overall losses in other configurations become smaller than that in the reference coil. Compared with the reference coil, the reductions of the overall loss in the nonmagnetic substrate-based coil with weak and strong magnetic disks and in the magnetic substrate-based coil with strong magnetic disks are 18.0, 49.2, and 40.6% at $I_0 = 40\text{A}$, respectively. This indicates that strong magnetic disks still work well on reducing the overall loss, even including the hysteresis loss in ferromagnetic disks.

In addition, a comparative analysis on the nonmagnetic substrate-based coil with and without strong magnetic disks is carried out in the external-field case. The AC loss of the pancake coils with and without strong magnetic disks under the conditions of $B_{app} = 0$ and 0.5T is presented in Fig. 9. It

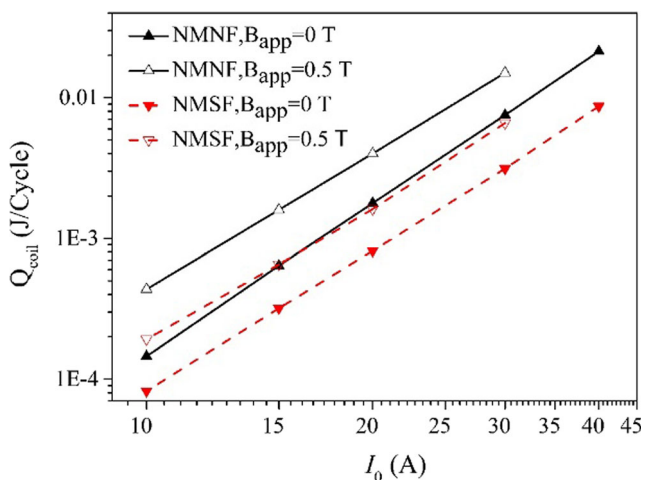


Fig. 9 The AC loss of nonmagnetic substrate-based coils with and without strong magnetic disks under the conditions of $B_{app} = 0$ and 0.5T

is clear that the axial background field of 0.5T enhances the AC loss of the coil to two to three times compared to the case of self-field. However, both in the self-field and external-field cases, the coil with strong magnetic disks has a smaller loss than the one without strong magnetic disks. For the self-field scenario, the AC loss of the coil with strong magnetic disks is 45.9% of the identical coil without strong magnetic disks at $I_0 = 20\text{A}$. While for the external-field scenario, the proportion declines relatively, saying 40.4%. The reason is that a large background field makes it easier for strong magnetic disks to be saturated, while unsaturated strong magnetic disks have a greater efficiency on reducing the AC loss of the coil.

Notably, for the external-field scenario, the shape of magnetization loop for strong magnetic disks is biased due to the interaction of the background field and the self-field induced by flowing current. Equation (14) used for hysteresis loss calculation is inapplicable. Therefore, we cannot accurately estimate the AC loss of magnetic substrate-based coil in the external-field scenario. Either the corresponding experiment or a complicated numerical study is needed to be carried out in the future work for calculating the hysteresis loss of ferromagnetic materials in that complicated case.

The detailed mechanism about the effect of ferromagnetic disks on the AC loss reduction needs research. Hence, we carry out a comparative analysis on the nonmagnetic substrate-based coils with and without strong magnetic disks in the self-field. Two sizes of strong magnetic disks with $dw = 0$ and 4mm are used for a better comparison. The AC loss in superconducting layers per turn for the

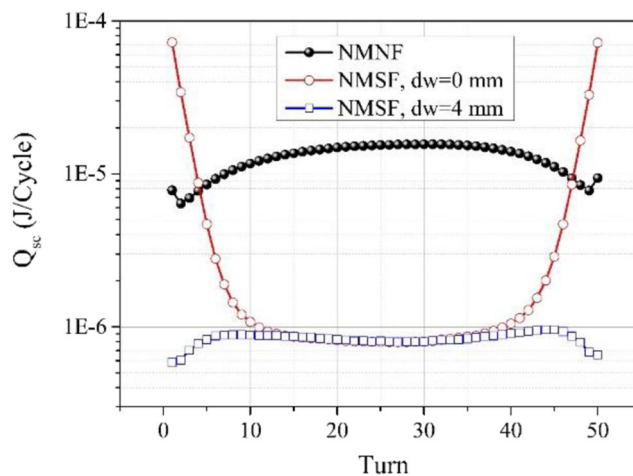
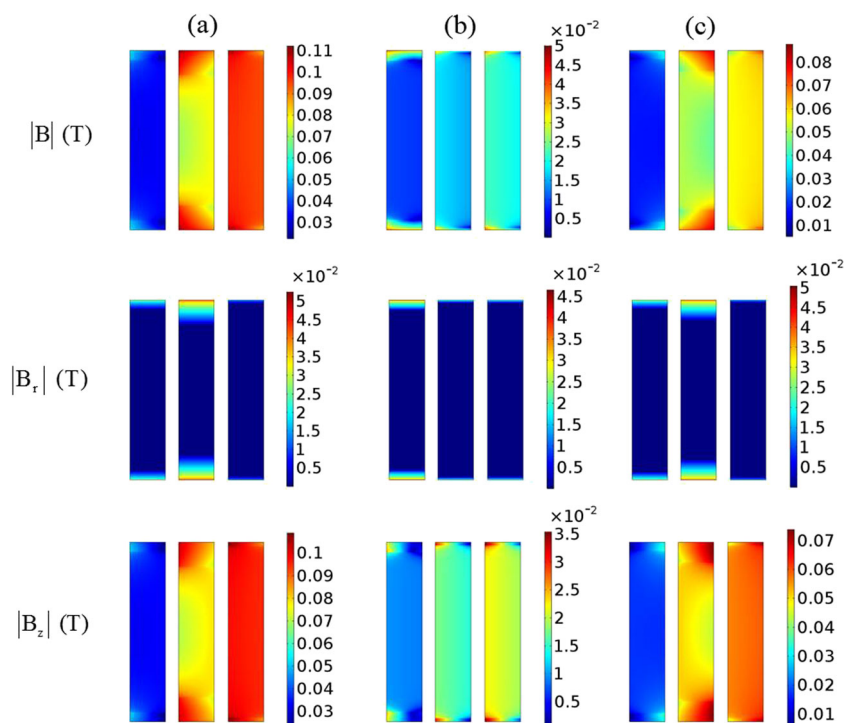


Fig. 10 The AC loss in superconducting layers per turn for nonmagnetic substrate-based coils with and without strong magnetic disks. The simulation uses two sizes of strong magnetic disks with $dw = 0$ and 4mm for a comparison. The red line with open circle symbol represents the case that ferromagnetic disks extend 0mm to both sides of the coil. The blue line with open square symbol represents the case that ferromagnetic disks extend 4mm to both sides of the coil

Fig. 11 The magnitude distributions of magnetic field (the upper row), radial field component (the middle row), and axial field component (the lower row) in three representative superconducting layers for nonmagnetic substrate-based coils without strong magnetic disks (left in each pair), with strong magnetic disks extending 0 mm to both sides of the coil (middle in each pair), and with strong magnetic disks extending 4 mm to both sides of the coil (right in each pair) at $t = 3T/2$ and $I = I_0 = 15A$. The three columns of the figure denote **a** the innermost turn, **b** the middle turn, and **c** the outermost turn, respectively. The thickness of the superconducting layers is thickened artificially for visual clarity



nonmagnetic substrate-based coils with and without strong magnetic disks is presented in Fig. 10. The corresponding magnetic field distribution in three representative superconducting layers is given in Fig. 11 at the moment $t = 3T/2$ with $I_0 = 15A$.

One can see from Fig. 10 that for nonmagnetic substrate-based coil without strong magnetic disks, the superconducting layers in the middle turns tend to suffer more AC loss than those in the inner and outer turns. While for the coil with strong magnetic disks extending 0 mm to both sides of the coil, compared to the case without strong magnetic disks, the AC loss of superconducting layers drops in the middle turns and rises in the inner and outer turns. While for the coil with strong magnetic disks extending 4 mm to both sides of the coil, the AC loss of superconducting layer in each turn decreases. Such phenomenon can be understood by the magnetic flux distribution plotted in Fig. 11. As can be seen from Fig. 11, though the magnetic field in each turn is increased by strong magnetic disks, the radial field component in middle turns is depressed and the radial field component in each turn is reduced by wider strong magnetic disks. It is known that the AC loss caused by perpendicular field component is greatly larger than that caused by the same amount of the parallel field component for REBCO CC tapes. Therefore, the reduction of the AC loss caused by strong magnetic disks is achieved by reducing the radial magnetic field. And, the wider strong magnetic disks can lower the AC loss more.

4 Conclusions

In this paper, with the self-consistent model based on the **A**-formulation and the finite element model built on the **H**-formulations, we explore the influences of the weak and strong magnetic disks on DC and AC characteristics of the nonmagnetic substrate-based coil and magnetic substrate-based coil. Both the self-field and external-field cases are analyzed. According to the numerical simulation results, several conclusions are obtained:

1. The ferromagnetic disks increase the magnetic field in superconducting layers and therefore lower the critical current of the pancake coils with magnetic substrates or not. The presence of background field weakens the effects of the ferromagnetic disks on critical current and AC loss of pancake coils.
2. For the nonmagnetic substrate-based coil, more than 95% of the AC loss in the coil comes from the AC loss in superconducting layers. Strong magnetic disks perform better than weak magnetic disks, which can reduce half of the AC loss in the coil. Even including the hysteresis loss in strong magnetic disks, the overall loss in the coil still drops at large current.
3. For the magnetic substrate-based coil with ferromagnetic disks, more than 90% of the AC loss in the coil comes from the AC loss in superconducting layer at large current. Strong magnetic disks can reduce the

overall loss in the coil at large current, while the weak magnetic disks are the opposite.

- The reduction of AC loss caused by ferromagnetic disks is attributed to the reduction of the radial field component in superconducting layers of pancake coil. This conclusion gives us a reminder on the optimization of the ferromagnetic disk's shape.

To be noted, the magnetic permeability of the ferromagnetic materials and the AC loss of the pancake coil are both related to the frequency of the AC transport current and temperature field [55, 56], which are not taken into account in this paper. However, we will develop the electromagnetic-thermal coupling model, which is used to analyze the effect of the flux diverter on the performances of pancake coils at different ambient temperatures. Furthermore, neither the geometrical factors [57] of different configurations nor the direct correlation between geometrical factors and AC loss is considered here. We will consider the influence of geometrical factors on the AC loss in our next work.

Funding Information The authors acknowledge the supports from the National Natural Science Foundation of China (nos. 11327802 and 11472120), 111 Project (B14044), the Fundamental Research Funds for the Central Universities (Izujbky-2017-k18), and the China Postdoctoral Science Foundation (no. 2017M610064).

References

- Yang, Y., Duan, S., Ren, Y., Jiang, Y., Feng, L., Zhang, X., Chai, H., Kuang, M., Wu, J., Yang, X.: Design and development of a cryogen-free superconducting prototype generator with YBCO field windings. *IEEE Trans. Appl. Supercond.* **26**, 1 (2016)
- Ali, M.H., Wu, B., Dougal, R.A.: An overview of SMES applications in power and energy systems. *IEEE Trans. Sustain. Energy* **1**, 38 (2010)
- Pan, A.V., MacDonald, L., Baiej, H., Cooper, P.: Theoretical consideration of superconducting coils for compact superconducting magnetic energy storage systems. *IEEE Trans. Appl. Supercond.* **26**, 1 (2016)
- Weijers, H.W., Trociewitz, U.P., Markiewicz, W.D., Jiang, J., Myers, D., Hellstrom, E.E., Xu, A., Jaroszynski, J., Noyes, P., Viouchkov, Y., Larbalestier, D.C.: High field magnets with HTS conductors. *IEEE Trans. Appl. Supercond.* **20**, 576 (2010)
- Van der Laan, D.C., Lu, X., Goodrich, L.F.: Compact GdBa₂Cu₃O_{7- δ} coated conductor cables for electric power transmission and magnet applications. *Supercond. Sci. Technol.* **24**, 042001 (2011)
- Liu, G., Zhang, G., Jing, L., Yu, H., Ai, L., Yuan, W., Li, W.: Influence of substrate magnetism on frequency-dependent transport loss in HTS-coated conductors. *IEEE Trans. Appl. Supercond.* **27**, 1 (2017)
- Rupich, M.W., Verebelyi, D.T., Zhang, W., Kodenkandath, T., Li, X.: Metalorganic deposition of YBCO films for second-generation high-temperature superconductor wires. *MRS Bull.* **29**, 572 (2004)
- Hazelton, D.W., Selvamani, V., Duval, J.M., Larbalestier, D.C., Markiewicz, W.D., Weijers, H.W., Holtz, R.L.: Recent developments in 2G HTS coil technology. *IEEE Trans. Appl. Supercond.* **19**, 2218 (2009)
- Xia, J., Bai, H., Lu, J., Gavrilin, A.V., Zhou, Y., Weijers, H.W.: Electromagnetic modeling of REBCO high field coils by the H-formulation. *Supercond. Sci. Technol.* **28**, 125004 (2015)
- Polak, M., Usak, E., Jansak, L., Demencik, E., Levin, G.A., Barnes, P.N., Wehler, D., Moenter, B.: Coupling losses and transverse resistivity of multifilament YBCO coated superconductors. *J. Phys.: Conf. Ser.* **43**, 591 (2006)
- Carr, W., Oberly, C.: Filamentary YBCO conductors for AC applications. *IEEE Trans. Appl. Supercond.* **9**, 1475 (1999)
- Lakshmi, L.S., Thakur, K.P., Staines, M.P., Badcock, R.A., Long, N.J.: Magnetic AC loss characteristics of 2G Roebel cable. *IEEE Trans. Appl. Supercond.* **19**, 3361 (2009)
- Grilli, F., Zermeño, V., Vojenčiak, M., Pardo, E., Kario, A., Goldacker, W.: AC losses of pancake coils made of Roebel cable. *IEEE Trans. Appl. Supercond.* **23**, 5900205 (2013)
- Levin, G.A., Barnes, P.N.: Concept of multiply connected superconducting tapes. *IEEE Trans. Appl. Supercond.* **15**, 2158 (2005)
- Ainslie, M.D., Yuan, W., Flack, T.J.: Numerical analysis of AC loss reduction in HTS superconducting coils using magnetic materials to divert flux. *IEEE Trans. Appl. Supercond.* **23**, 4700104 (2013)
- Farinon, S., Fabbriatore, P., Gomory, F., Greco, M., Seiler, E.: Modeling of current density distributions in critical state by commercial FE codes. *IEEE Trans. Appl. Supercond.* **15**, 2867 (2005)
- He, A., Xue, C., Yong, H., Zhou, Y.: Effect of soft ferromagnetic substrate on ac loss in 2G HTS power transmission cables consisting of coated conductors. *Supercond. Sci. Technol.* **27**, 025004 (2014)
- Wan, X.X., Huang, C.G., Yong, H.D., Zhou, Y.H.: Effect of the magnetic material on AC losses in HTS conductors in AC magnetic field carrying AC transport current. *AIP Adv.* **5**, 117139 (2015)
- Yong, H., Zhao, M., Jing, Z., Zhou, Y.: Effect of shear stress on electromagnetic behaviors in superconductor-ferromagnetic bilayer structure. *J. Appl. Phys.* **116**, 123911 (2014)
- Ma, G.-T.: Hysteretic ac loss in a coated superconductor subjected to oscillating magnetic fields: ferromagnetic effect and frequency dependence. *Supercond. Sci. Technol.* **27**, 065011 (2014)
- Krüger, P., Grilli, F., Vojenčiak, M., Zermeño, V.M.R., Demencik, E., Farinon, S.: Superconductor/ferromagnet heterostructures exhibit potential for significant reduction of hysteretic losses. *Appl. Phys. Lett.* **102**, 202601 (2013)
- Gömöry, F., Vojenčiak, M., Pardo, E., Solovyov, M., Šouc, J.: AC losses in coated conductors. *Supercond. Sci. Technol.* **23**, 034012 (2010)
- Gömöry, F., Vojenčiak, M., Pardo, E., Šouc, J.: Magnetic flux penetration and AC loss in a composite superconducting wire with ferromagnetic parts. *Supercond. Sci. Technol.* **22**, 034017 (2009)
- Majoros, M., Glowacki, B.A., Campbell, A.M.: Transport ac losses and screening properties of Bi-2223 multifilamentary tapes covered with magnetic materials. *Physica C* **338**, 251 (2000)
- Ogawa, J., Fukui, S., Oka, T., Sakurai, T., Sano, Y., Tada, H., Yoshii, Y.: Experimental investigation of AC loss characteristics of stacked HTS Tapes in an iron core. *IEEE Trans. Appl. Supercond.* **26**, 1 (2016)
- Lai, L., Gu, C., Qu, T., Zhang, M., Li, Y., Liu, R., Coombs, T., Han, Z.: Simulation of AC loss in small HTS coils with iron core. *IEEE Trans. Appl. Supercond.* **25**, 1 (2015)
- Pardo, E., Šouc, J., Vojenčiak, M.: AC loss measurement and simulation of a coated conductor pancake coil with ferromagnetic parts. *Supercond. Sci. Technol.* **22**, 075007 (2009)
- Ainslie, M.D., Hu, D., Zou, J., Cardwell, D.A.: Simulating the in-field AC and DC performance of high-temperature superconducting coils. *IEEE Trans. Appl. Supercond.* **25**, 1 (2015)

29. Liu, G., Zhang, G., Jing, L., Yu, H.: Numerical study on AC loss reduction of stacked HTS tapes by optimal design of flux diverter. *Supercond. Sci. Technol.* **30**, 125014 (2017)
30. Suenaga, M., Li, Q.: Effects of magnetic substrates on ac losses of YBa₂Cu₃O₇ films in perpendicular ac magnetic fields. *Appl. Phys. Lett.* **88**, 262501 (2006)
31. Mawatari, Y.: Magnetic field distributions around superconducting strips on ferromagnetic substrates. *Phys. Rev. B* **77**, 104505 (2008)
32. Sanchez, A., Del-Valle, N., Navau, C., Chen, D.X.: Influence of magnetic substrate in the transport critical current of superconducting tapes. *Appl. Phys. Lett.* **97**, 072504 (2010)
33. Zhang, M., Kvitkovic, J., Kim, J.H., Kim, C., Pamidi, S., Coombs, T.: Alternating current loss of second-generation high-temperature superconducting coils with magnetic and non-magnetic substrate. *Appl. Phys. Lett.* **101**, 102602 (2012)
34. Zhang, M., Kvitkovic, J., Kim, J.H., Kim, C.H., Pamidi, S.V., Coombs, T.A.: Alternating current loss of second-generation high-temperature superconducting coils with magnetic and non-magnetic substrate. *Appl. Phys. Lett.* **101**, 102602 (2012)
35. Šouc, J., Pardo, E., Vojenčiak, M., Gömöry, F.: Theoretical and experimental study of AC loss in high temperature superconductor single pancake coils. *Supercond. Sci. Technol.* **22**, 015006 (2008)
36. Genenko, Y.A., Snezhko, A., Freyhardt, H.C.: Overcritical states of a superconductor strip in a magnetic environment. *Phys. Rev. B* **62**, 3453 (2000)
37. Erdogan, M., Tunc, S., Inanir, F.: AC loss analysis of HTS pancake coil of coated superconductors with ferromagnetic substrate. *J. Supercond. Novel. Magn.* **30**, 1993 (2016)
38. Li, S., Chen, D.X., Fang, J.: Transport ac losses of a second-generation HTS tape with a ferromagnetic substrate and conducting stabilizer. *Supercond. Sci. Technol.* **28**, 125011 (2015)
39. Ainslie, M.D., Flack, T.J., Campbell, A.M.: Calculating transport AC losses in stacks of high temperature superconductor coated conductors with magnetic substrates using FEM. *Physica C* **472**, 50 (2012)
40. Zermeno, V.M., Abrahamsen, A.B., Mijatovic, N., Jensen, B.B., Sørensen, M.P.: Calculation of alternating current losses in stacks and coils made of second generation high temperature superconducting tapes for large scale applications. *J. Appl. Phys.* **114**, 173901 (2013)
41. Thakur, K.P., Raj, A., Brandt, E.H., Kvitkovic, J., Pamidi, S.V.: Frequency-dependent critical current and transport ac loss of superconductor strip and Roebel cable. *Supercond. Sci. Technol.* **24**, 065024 (2011)
42. Haynes, W.M.: *CRC Handbook of Chemistry and Physics*. CRC Press, Boca Raton (2014)
43. Lu, J., Choi, E.S., Zhou, H.D.: Physical properties of Hastelloy[®]C-276[™] at cryogenic temperatures. *J. Appl. Phys.* **103**, 064908 (2008)
44. Lakshmi, L.S., Staines, M.P., Badcock, R.A., Long, N.J., Majoros, M., Collings, E.W., Sumption, M.D.: Frequency dependence of magnetic ac loss in a Roebel cable made of YBCO on a Ni–W substrate. *Supercond. Sci. Technol.* **23**, 085009 (2010)
45. Zermeno, V., Sirois, F., Takayasu, M., Vojenciak, M., Kario, A., Grilli, F.: A self-consistent model for estimating the critical current of superconducting devices. *Supercond. Sci. Technol.* **28**, 085004 (2015)
46. Zermeno, V.M., Quaiyum, S., Grilli, F.: Open-source codes for computing the critical current of superconducting devices. *IEEE Trans. Appl. Supercond.* **26**, 1 (2016)
47. Liu, D., Xia, J., Yong, H., Zhou, Y.: Estimation of critical current distribution in Bi₂Sr₂CaCu₂O_x cables and coils using a self-consistent model. *Supercond. Sci. Technol.* **29**, 065020 (2016)
48. Miyagi, D., Yunoki, Y., Umabuchi, M., Takahashi, N., Tsukamoto, O.: Measurement of magnetic properties of Ni-alloy substrate of HTS coated conductor in LN₂. *Physica C* **468**, 1743 (2008)
49. Nguyen, D.N., Ashworth, S.P., Willis, J.O., Sirois, F., Grilli, F.: A new finite-element method simulation model for computing AC loss in roll assisted biaxially textured substrate YBCO tapes. *Supercond. Sci. Technol.* **23**, 025001 (2010)
50. Brambilla, R., Grilli, F., Martini, L.: Development of an edge-element model for AC loss computation of high-temperature superconductors. *Supercond. Sci. Technol.* **20**, 16 (2007)
51. Hong, Z., Campbell, A.M., Coombs, T.A.: Numerical solution of critical state in superconductivity by finite element software. *Supercond. Sci. Technol.* **19**, 1246 (2006)
52. Sirois, F., Dione, M., Roy, F., Grilli, F., Dutoit, B.: Evaluation of two commercial finite element packages for calculating AC losses in 2-D high temperature superconducting strips. *J. Phys.: Conf. Ser.* **97**, 012030 (2008)
53. Kajikawa, K., Hayashi, T., Yoshida, R., Iwakuma, M., Funaki, K.: Numerical evaluation of AC losses in HTS wires with 2D FEM formulated by self magnetic field. *IEEE Trans. Appl. Supercond.* **13**, 3630 (2003)
54. Xia, J., Yong, H., Zhou, Y.: Numerical simulations of the alternating current loss in round high-temperature superconducting wire with a hole defect. *J. Appl. Phys.* **114**, 093905 (2013)
55. Bishop, J.: Tables of the frequency dependence of permeability for the Polivanov domain model. *J. Phys. D: Appl. Phys.* **4**, 1235 (1971)
56. Samantaray, B., Singh, A.K., Perumal, A., Ranganathan, R., Mandal, P.: Spin dynamics and frequency dependence of magnetic damping study in soft ferromagnetic FeTaC film with a stripe domain structure. *AIP Adv.* **5**, 067157 (2015)
57. Zola, D., Gömöry, F., Polichetti, M., Strýček, F., Seiler, E., Hušek, I., Kováč, P., Pace, S.: A study of coupling loss on bi-columnar BSCCO/Ag tapes through ac susceptibility measurements. *Supercond. Sci. Technol.* **17**, 501 (2004)